Journal of Applied Polymer Science

Positron annihilation and other experimental studies on polycarbonate/MPDMAPP nanocomposite

Sheela Thimmaiah,[1] Rajashekhar Fakeerappa Bhajantri,[2] Padinharu Madathil Gopalakrishnan Nambissan,[3] Ravindrachary Vasachar,[1] Sunil Gurunath Rathod,[1] Boja Poojary[4]

[1]Department of Physics, Mangalore University, Mangalagangotri 574 199, Karnataka, India
[2]Department of Physics, Karnatak University, Dharwad 580 003, Karnataka, India
[3]Applied Nuclear Physics Division, Saha Institute of Nuclear Physics, Bidhannagar, Kolkata700 064, West Bengal, India
[4]Department of Chemistry, Mangalore University, Mangalagangotri 574 199, Karnataka, India
Correspondence to: R.F. Bhajantri (E-mail: rfbhajantri@kud.ac.in or rfbhajantri@gmail.com)

ABSTRACT: The composite films of polycarbonate (PC) filled with 1-(4-methylphenyl)-3-(4-N,N-dimethylaminophenyl)-2-propen-1-one (MPDMAPP) were prepared by solution casting. The *FT-IR* results of the prepared films confirmed the hydrophobic and dipole-dipole interaction between PC and MPDMAPP, which is a major driving force for the formation of charge transfer complex (CTC). *UV*–Vis absorption spectra showed three peaks and the optical band gap E_g for pure PC is 4.31 eV which decreased to 4.1 eV after 15 *wt %* doping. The fluorescence spectral results show a strong emission and quenching in the wavelength region 510 *to* 550 nm for 408 nm excitation due to increase in amorphousness, which is observed in X-ray diffraction (XRD) results. The decrease in ortho-positronium (o-Ps) lifetime τ_3 and corresponding intensity I_3 from positron annihilation lifetime spectroscopy (PALS) and the S-parameter from Doppler broadening measurements show both inhibition and quenching of Ps formation in the PC/MPDMAPP composite due to the presence of dimethylamino $N(CH_3)_2$ group. The mechanical properties such as Young's modulus, tensile strength, and stiffness increase with doping concentration and confirmed that the composite films are mechanically stable. The growth of nanostructures of MPDMAPP within PC films is studied with SEM and TEM images and confirms the uniform dispersion and interaction between the functional groups of PC and MPDMAPP. © 2015 Wiley Periodicals, Inc. J. Appl. Polym. Sci. **2015**, *132*, 42053.

KEYWORDS: composites; mechanical properties; nanoparticles; nanowires and nanocrystals; optical properties; polycarbonates

Received 3 November 2014; accepted 29 January 2015
DOI: 10.1002/app.42053

INTRODUCTION

In recent years, polymer-based nanocomposite materials have played a very important role in scientific and technological areas; because of their wide spread applications in photonics, biotechnology, and optoelectronics in comparison with other classes of engineering materials.[1,2] Contemporary advancements in modern science and technology require large number of organic photochromic materials with high quality and good responses for numerous optical device applications.[3,4] This is mainly due to advantages related to their light weight, good mechanical strength, and excellent optical properties, which make them as multifunctional materials. In order to achieve improved processing, optical effect, and reduction of cost, the organic fluorescent chromophores are either embedded or cross-linked into polymer matrix to achieve guest-host complexes to acquire suitable properties.[5,6]

Polycarbonate (PC) is an amorphous engineering thermoplastic polymer with good physical and chemical properties, excellent transparency, light weight, high mechanical strength, good thermal stability, and high heat distortion temperature. It can be doped with carbon nanofibres, organic chromophore nanoparticles for optical devices of diverse applications, because it provides uniformity and greater stability for distribution of nanoparticles. The doping will modify the chemical structure and properties to suit the specific purpose.[7–9] The chalcone derivatives are noticeable materials for their excellent blue light transmittance. Polymers embedded with chalcone derivatives normally show good optical properties, fluorescence polarization, color change, fluorescent complex formation, and photochromism.[2,4]

Polymers contain the atomic and molecular scale free volumes that arise because of irregular molecular packing in amorphous phase and hence molecular relaxation of the polymer chains and terminal ends; play an important role in determining their optical, physical, chemical, and microstructural properties. Positron annihilation spectroscopy (PAS) is a well-established

technique to detect directly the existence of free-volume holes and their distribution in polymeric materials, and has attracted much attention in polymer physics.[10,11] When an energetic positron (of end point energy 540 keV) from a radioactive source (^{22}Na, in this case) enters a condensed medium like a polymer, it thermalizes by losing its energy in a very short time and the process requires a few ps. It then annihilates with an electron of the medium by a free annihilation process or the positron is trapped in a defect site and annihilates with an electron of the defect site or forms a bound state called the positronium atom (Ps) with one of the surrounding electrons. Usually Ps exists in two spin states, a para-positronium (p-Ps, particle spins antiparallel) which annihilates with a lifetime of 0.125 ns and ortho-positronium (o-Ps, particle spins parallel) which decays with a lifetime of 142 ns in vacuum. In materials media including polymers, the Ps localizes in the free volume holes and there is a finite probability that the positron of o-Ps bound state may annihilate with a molecular electron of opposite spin, rather than its bound partner. This process is known as o-Ps pick-off annihilation and hence the lifetime of o-Ps (typically observed as τ_3) gets reduced to a few ns. The o-Ps annihilation rate (λ) in terms of free volume radius R in polymers is given by the eq. (1).

$$\lambda=(\tau_3)^{-1}=2\left[1-\frac{R}{R_0}+\frac{1}{2\pi}\sin\left(\frac{2\pi R}{R_0}\right)\right] \quad (1)$$

Here $R_0 = R + \Delta R$, where ΔR =1.66 Å is an empirical fitting parameter[12] which represents the thickness of electron layer around the hole, λ is expressed in ns^{-1} and τ_3 is expressed in ns.

Ps is the lightest atom that can chemically react with molecules and different functional groups by two processes, *viz.*, chemical quenching, which decreases the o-Ps lifetime and chemical inhibition, which decreases the probability of o-Ps formation (typically observed as I_3). Polymers are mainly structured with carbon and hydrogen, doped with polar groups such as halogen and nitrogen, which forms the charge transfer complex (CTC) and is expected to inhibit and quench the o-Ps formation.[13,14] Doppler broadening spectroscopic (DBS) measurements on the other hand can provide information about the polar groups and chemical surrounding of nanoholes in polymers. The width and shape of the 511 keV annihilation line yields the information about the electrons with which the positrons annihilate.[15]

Yet another aspect that we focused our attention on in this work is fluorescence quenching and emission. In our earlier article, we have reported PALS results of MPDMAPP chalcone chromophore doped PVA and showed that the formation of CTCs alter the microstructural properties of PVA.[6] In another article,[2] we have also reported about the photochromic nature in fluorescence emission properties of MPDMAPP doped PVA/PVP blend due to intermolecular hydrogen bonding and formation of CTCs. The UV–Vis absorption spectroscopy is an important tool to study the optical transitions and to obtain information about the optical band gap in polymeric materials. Fluorescence spectroscopy is a powerful, sensitive, and nondestructive tool to understand the intra/intermolecular energy transfer, chemical behaviors of the macromolecules, molecular configuration, and aggregation in polymer nanocomposites.

In the present investigation, the nanocomposite films of polycarbonate doped with a chalcone derivative were prepared using solution casting. The fluorescence quenching and increase in emission wavelength with increase in doping level is investigated. The chemical, microstructural, optical, mechanical, and morphological properties were studied using Fourier transform-infrared (FT-IR), UV–Vis, and fluorescence spectroscopy, X-ray diffraction, universal testing machine (UTM), scanning electron microscope (SEM) and transmission electron microscope (TEM). The inhibition and quenching of positronium formation in PC/MPDMAPP nanocomposites have been investigated using PAS and DBS.

EXPERIMENTAL

The polycarbonate (PC) used in this work was obtained from Sigma-Aldrich, Bangalore. The newly synthesized organic compound 1-(4-methylphenyl)-3-(4-*N*,*N*-dimethylaminophenyl)-2-propen-1-one (MPDMAPP) is used for doping into PC. The PC/MPDMAPP composite films were prepared using solution casting method in dichloromethane solvent.[2] The thicknesses of the films are in the range of 80 to 110 μm measured using Mitutoyo-7327 dial thickness gauge with accuracy of 0.001 mm. The FT-IR spectra of the composites were obtained by KBr pellet method using Shimadzu IR Prestige-2 spectrometer in the wavenumber range 400 to 4000 cm^{-1}. UV–Visible absorption spectra were recorded using Shimadzu-1800 spectrophotometer in the wavelength range 190 to 800 nm. The X-ray diffraction (XRD) patterns of the samples were recorded using Rigaku Miniflex-II bench top XRD using Ni-filtered Cu-K_α radiation of wavelength 1.5406 Å and graphite monochromator, scanned in the 2θ range of 5° to 50° with a scanning speed of 1° per min and step size of 0.02°.

The fluorescence spectra were recorded using Jobin Yvon Flurolog-3–11 spectrofluorometer with 500 W Xenon lamp to excite the sample at 408 nm. The Fluorescence microscopic images were taken with Olympus BX-60. The mechanical properties of the composite films were measured with Lloyd LRX plus universal testing machine (UTM) equipped with 5 kN load cell and by using the sample size of 50 mm x 25 mm with a constant rate of 25 mm/min and gauge length of 50 mm. Scanning electron microscopy (SEM) images were taken with JEOL model JSM-6390LV at an acceleration voltage of 30 KV and images were scanned in WD 8 mm, SEI mode. Transmission electron microscopy (TEM) images of the samples were taken using 120 kV Hitachi (H-7500) instrument operating at an acceleration voltage of 100 kV. Samples for TEM were prepared by drop casting the MPDMAPP and PC/MPDMAPP dispersion onto the holey carbon film on a fine mesh Cu grid and letting it dry.

Positron annihilation lifetime(PAL) measurements were carried out at Saha Institute of Nuclear Physics (SINP), Kolkata, India, using a ^{22}Na source ($^{22}NaHCO_3$ source dissolved in dilute HCl acid) of approximate strength 400 kBq. The source was in the form of residual deposit on a thin (~2 mg cm^2) Ni foil and covered by an identical foil. The source correction was done during the positron lifetime data analysis for the contributions from those positrons getting annihilated in the Ni foil

($\tau_{s1} = 102$ ps) when the positrons try to penetrate through it. Absolute intensity of the positron annihilation within the Ni foil is calculated using the eq. (2).[16]

$$I_{foil} = \quad 0.324 Z^{0.93} d^{3.45 Z^{-0.41}} \qquad (2)$$

where Z is effective atomic number of the sample, and d is the foil thickness in mg/cm^2. The positron source was sandwiched between two stacks of the composite films ensuring that all positrons annihilate within the sample. The γ rays were detected using a slow-fast γ-γ coincidence setup consists of BaF_2 scintillators coupled to Phillips XP2020Q photomultiplier tubes. The coincidence spectrometer had time resolution function consisting of two Gaussians of FWHM 180 ps and 200 ps for the γ-rays from ^{60}Co source with relative intensities 90% and 10%, respectively. About 10^6 counts were collected under each spectrum and the analyses of positron lifetime data were carried out using the latest version of the PATFIT package namely PALSfit.[17] After subtracting the background and deconvoluting the resolution function, the spectra of all the samples were source-corrected and fitted satisfactorily with variances of fit $\sim 1.05 \pm 0.15$ to three-component exponential decay composed of lifetimes τ_1, τ_2, and τ_3 and with relative intensities I_1, I_2, and I_3. Doppler broadening spectrum was obtained using high purity germanium (HPGe) detector with a resolution of 1.28 keV FWHM at 511 keV. The usual shape parameter S was estimated by taking the ratio of the area under the central region (511 ± 0.64 keV) to the total area of the photo peak (511 ± 8 keV). S is representative of the annihilation of positrons with low momentum electrons.

RESULTS AND DISCUSSION

FT-IR Studies

The FT-IR spectra of pure PC, pure MPDMAPP, and PC/MPDMAPP composites are shown in Figure 1. The IR band of pure PC at 3057 cm^{-1} is assigned to aromatic C—H stretching. The bands at 2968 cm^{-1} and 2874 cm^{-1} are attributed to C—H asymmetric and symmetric stretching. The strong bands at 1776 cm^{-1} and 1504 cm^{-1} are due to carbonyl C=O and aromatic C=C stretching, respectively. The other bands are attributed as follows: the IR band at 1217 cm^{-1} is assigned to C—O—C stretching vibration and C—H wagging, 1013 cm^{-1} assigned to aromatic C—H in plane bending and 831 cm^{-1} to aromatic C—H out of plane bending.[17] Pure MPDMAPP shows characteristic bands at 1645 cm^{-1} assigned to carbonyl C=O stretching, 1554 cm^{-1} (C=C stretching), 1438 cm^{-1} (C—H def), the band at 812 cm^{-1} and 742 cm^{-1} assigned to aromatic C—H deformation.[18] The FT-IR spectral assignments of PC/MPDMAPP composite are as follows: the aromatic C—H stretching band shifts to 3059 cm^{-1}. The C—H asymmetric stretching band shifts to 2970 cm^{-1} and C—H symmetric stretching band shifts to 2874 cm^{-1}. The aromatic C=C stretching band shifts to 1502 cm^{-1}, C—O—C stretching and C—H wagging bands shift to 1205 cm^{-1}, aromatic C—H in plane bending shifts to 1013 cm^{-1} and aromatic C—H out of plane bending shifts to 831 cm^{-1}. These shifts in band positions and the variation in their intensities support the hydrophobic and dipole-dipole interaction between PC and MPDMAPP. The binding of MPDMAPP with PC through these interactions is

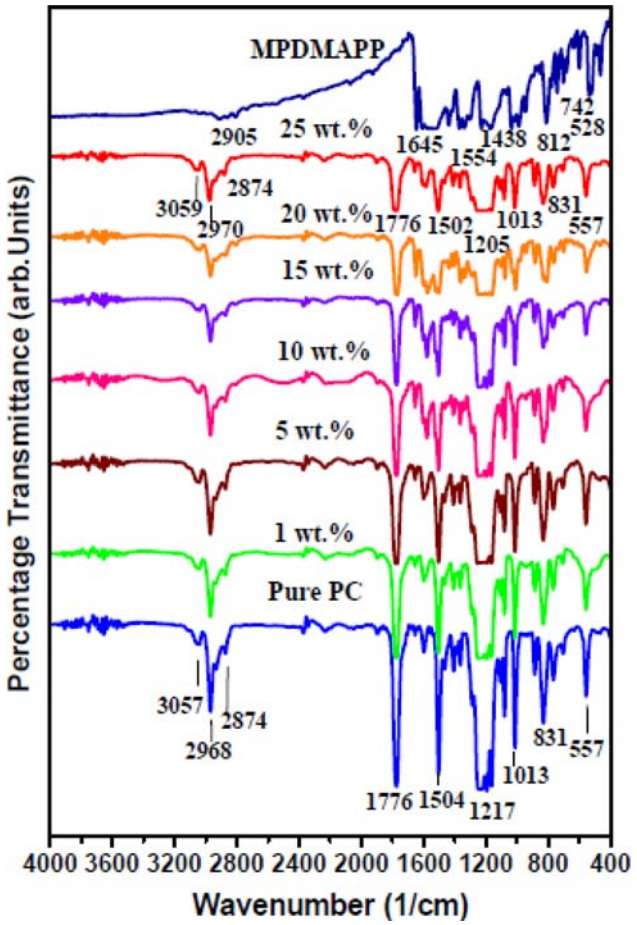

Figure 1. FT-IR Spectra of the pure PC and PC/MPDMAPP composites. [Color figure can be viewed in the online issue, which is available at wileyonlinelibrary.com.]

believed to be a major driving force for the formation of CTC,[2] as shown in Figure 2(a).

The hydrophobic interaction occurs between the dimethylamine $N(CH_3)_2$ group of MPDMAPP and the methyl groups (CH_3) of PC and *vice versa*. In addition to this, the dipole-dipole interaction also takes place between the carbonyl oxygen and carbonyl carbon of MPDMAPP and the carbonyl carbon of PC. Internal electron flow (charge transfer) in MPDMAPP occurs from *N,N*-dimethylamino group (donor site) to carbonyl group (acceptor site) through mesomeric effect, and from methyl group to carbonyl group through inductive effect, shown in the figure below. This internal electron flow is responsible for dipole-dipole interaction between MPDMAPP and PC.

The intermolecular charge transfer interaction between MPDMAPP and PC also reflected in the characteristic IR bands. This is mainly due to the fact that the chalcone MPDMAPP contains electron donating methyl group on one side and dimethyl amino group on the other side. The *N,N*-dimethylamino group releases electrons through mesomeric effect and methyl group transfers charge through inductive group to the attached phenyl rings, thus making them electron rich. On the other hand, charge dispersion also occurs in PC from phenyl

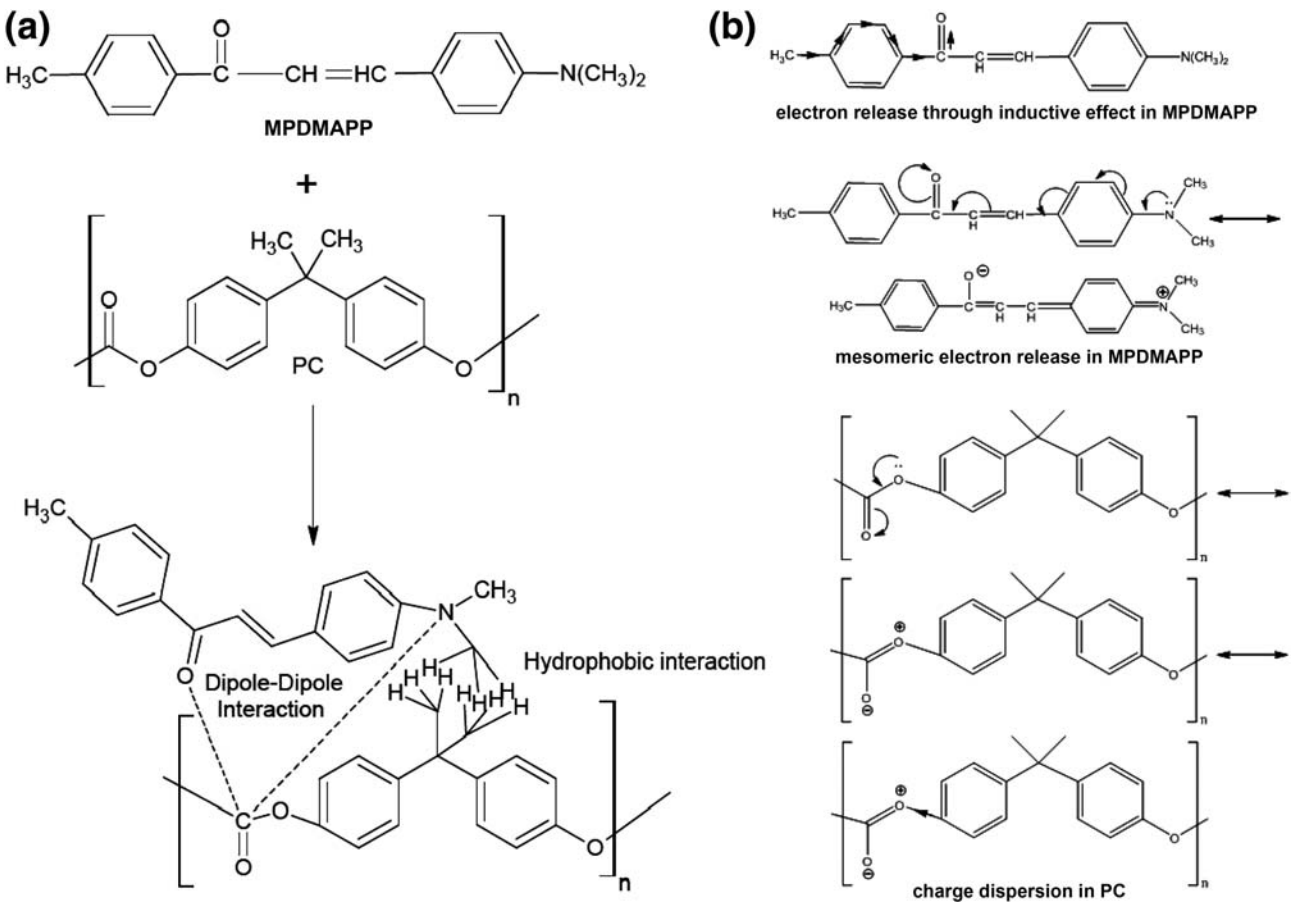

Figure 2. (a) Interactions between MPDMAPP & PC in the composite film. (b) Reaction scheme.

ring to carbonate group thus making the phenyl ring electron poor as shown in the Figure 2(b). This will lead to charge transfer interaction between MPDMAPP and PC.

The groups with a tendency of releasing electrons due to inductive or mesomeric effect will act as a donor site of the chalcone moiety and the groups with a tendency of accepting electrons either due to mesomeric or inductive effect will act as an acceptor site.[18,19] The charge transfer also takes place from the aromatic (benzene) π-electrons of the PC to the MPDMAPP carbonyl groups. This kind of charge transfer also occurs from the nonbonding electrons of $N(CH_3)_2$ groups present in MPDMAPP to carbonyl (C═O) groups of PC. All these interactions are reflected in the shifting of characteristic band positions (Figure 1). Further, the variation of band intensities in FT-IR spectra suggests that the chalcone chromophore (MPDMAPP) is interacting with PC matrix with the indicated electronic interactions between them.

UV–Visible and Optical Band Gap Studies

UV–visible absorption spectra of PC/MPDMAPP composite films are illustrated in Figure 3 and it is clear from the figure that the pure PC as well as PC/MPDMAPP composite films show two absorption peaks due to the presence of carbonyl group segments. The first peak at 220 nm assigned as localized $n\rightarrow\pi^*$ transition shifts to 223 nm upon MPDMAPP doping in PC. The second peak at 275 nm is assigned to $n\rightarrow\pi^*$ inter band transitions and this transition is attributed to the excitation in the aromatic rings and phenyl groups of MPDMAPP. The third peak at 407 nm is assigned to $\pi\rightarrow\pi^*$ transitions due to the presence of charge transfer (CT) groups within MPDMAPP, which is shifting to 408 nm upon doping.

It is observed from FT-IR results that the hydrophobic and dipole-dipole interactions cause the formation of CTCs, and therefore, both bathochromic and hyperchromic shifts in absorption are observed with increase in concentration of MPDMAPP within PC.[2] This variation is a symptom of disturbance in local structure and is expected due to the interaction of MPDMAPP with the host PC. When MPDMAPP molecules interact with the carbonyl group of PC, the electron density of the C═O bond is reduced, which causes the red-shift of the absorption peak and affects the optical energy band gap.[20]

To obtain more information about the band structure of PC/MPDMAPP matrix, the values of optical band gaps (E_g) are determined by the relationship between absorption coefficient $\alpha(v)$ and the optical band gap E_g, which obeys classical Tauc's expression.[21] To translate the absorption spectrum into Tauc's plot, the frequency-dependent absorption coefficient $\alpha(v) = \beta(hv - E_g)^r/hv$ given by Mott and Davis is used.[22] Here β is the band tailing parameter, a constant, and the exponent (r) is an

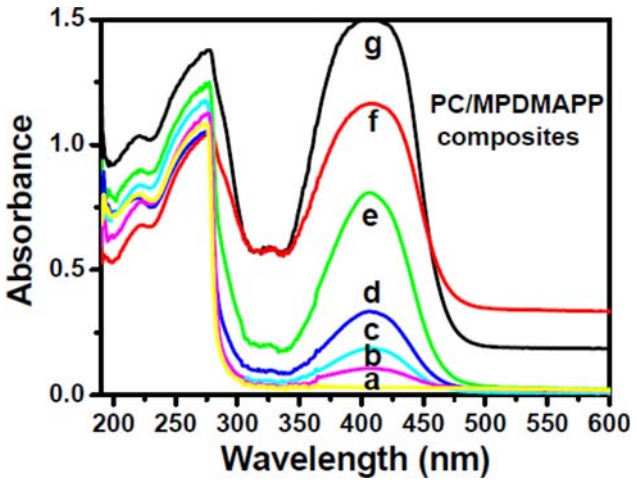

Figure 3. UV–Visible spectra of (a) pure PC, (b) 1 wt %, (c) 5 wt %, (d) 10 wt %, (e) 15 wt %, (f) 20 wt %, and (g) 25 wt % MPDMAPP doped composite films. [Color figure can be viewed in the online issue, which is available at wileyonlinelibrary.com.]

empirical index, which is equal to 2, 3, 1/2, and 1/3 corresponding to indirect allowed, indirect forbidden, direct allowed and direct forbidden transitions respectively.

The optical band gap E_g can be estimated by extrapolating the linear portion of the curve at the point $(\alpha h\nu)^{1/2} = 0$ on $h\nu$-axis [Figure 4(a)] and the variation of the estimated E_g for pure PC and different MPDMAPP doping concentrations in PC is shown in Figure 4(b). The calculated E_g for pure PC is 4.31 eV and it decreases with increase in MPDMAPP doping concentration reaching the least value of 4.1 eV for 15 wt % dopant concentration. The chalcone derivative MPDMAPP contains both electron donor $CH_3/N(CH_3)_2$ groups and electron-acceptor C═O groups and it forms CTCs when doped into PC matrix, resulting in the variation of both the absorption and band edge. These CTCs modify the band structure and create the additional defect levels within the band gap.

XRD Studies

The XRD patterns of pure and MPDMAPP doped PC are illustrated in Figure 5. The XRD pattern of pure PC shows amorphous halo positioned around $2\theta = 17^o$ and that of MPDMAPP doped PC show around 22^o for 1 wt % doping. The peak positions are shifting towards higher diffraction angles and decreases in intensity with increase in MPDMAPP dopant concentration. This indicates clearly that the PC/MPDMAPP composites are not crystallized and develop an amorphous phase due to complex formation during the interaction of MPDMAPP with PC.

Fluorescence Studies

The organic chalcone compound MPDMAPP in its pure form shows second harmonic generation (SHG) conversion efficiency of 0.8 times that of urea.[19] However, upon embedding this compound into polymers like poly(methylmethacrylate) (PMMA),[23] poly(vinyl alcohol) (PVA),[2,4] the composite films are not showing second harmonic behavior, instead these composite films are showing fluorescent properties upon excitation with UV light. The essential requirement for a molecule to show second harmonic is the presence of electron donating groups on one end and electron withdrawing groups in the other end. The chalcone compound MPDMAPP, containing *N,N*-dimethylamino $[N(CH_3)_2]$ group acts as donor due to its strong mesomeric electron releasing behavior. The carbonyl group (C═O) acts as acceptor and it is connected with *N,N*-dimethylamino group through conjugated system. Similarly, in the present study also we observed fluorescent property when MPDMAPP is doped into PC. Since the chalcone MPDMAPP forms the charge transfer complex with PC, the electrons of electron donating *N,N*-dimethylamino group are involved in the formation of CTC, are not available for delocalization towards carbonyl group to exhibit NLO property. Thus, polymers which form CTC with chalcones may not exhibit NLO property.

The steady state fluorescence spectra of the PC/MPDMAPP composite films under the excitation wavelength of 408 nm are shown in Figure 6(i) and the variations of fluorescence peak wavelengths and intensities as a function of MPDMAPP dopant concentration are shown in Figure 6(ii). The fluorescence emission peaks in the green region are showing bathochromic shift from 510 nm for 1 wt % to 519, 534, 545, and 550 nm for 5, 10, 20, and 25 wt % doping concentrations respectively, whose intensity increases up to 5 wt % doping and then decreases for higher dopant concentration.

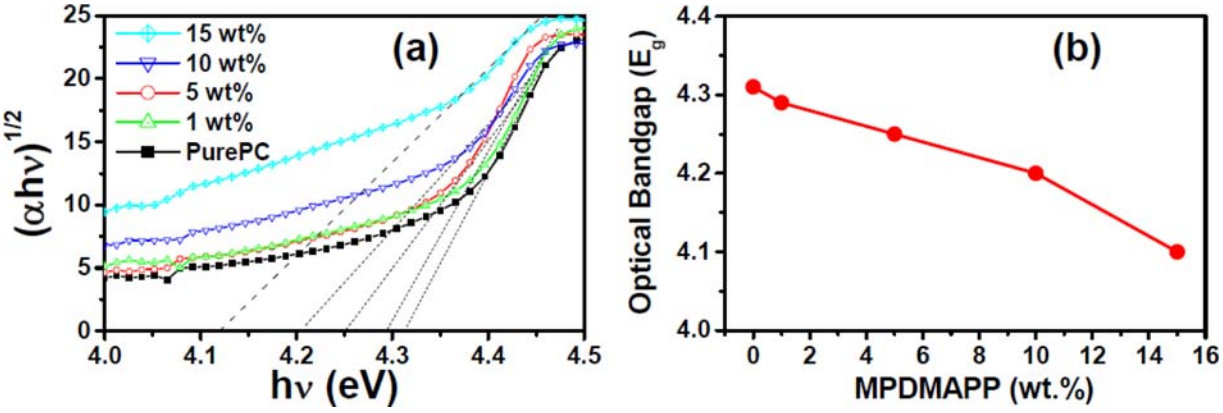

Figure 4. (a) Variation of $(\alpha h\nu)^{1/2}$ versus $h\nu$ and (b) optical band gap versus MPDMAPP dopant concentration. [Color figure can be viewed in the online issue, which is available at wileyonlinelibrary.com.]

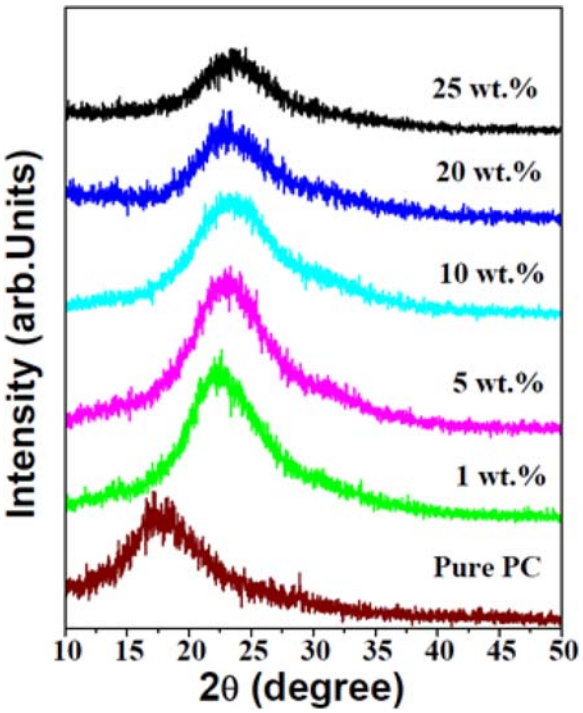

Figure 5. X-ray diffraction patterns of pure and MPDMAPP doped PC films. [Color figure can be viewed in the online issue, which is available at wileyonlinelibrary.com.]

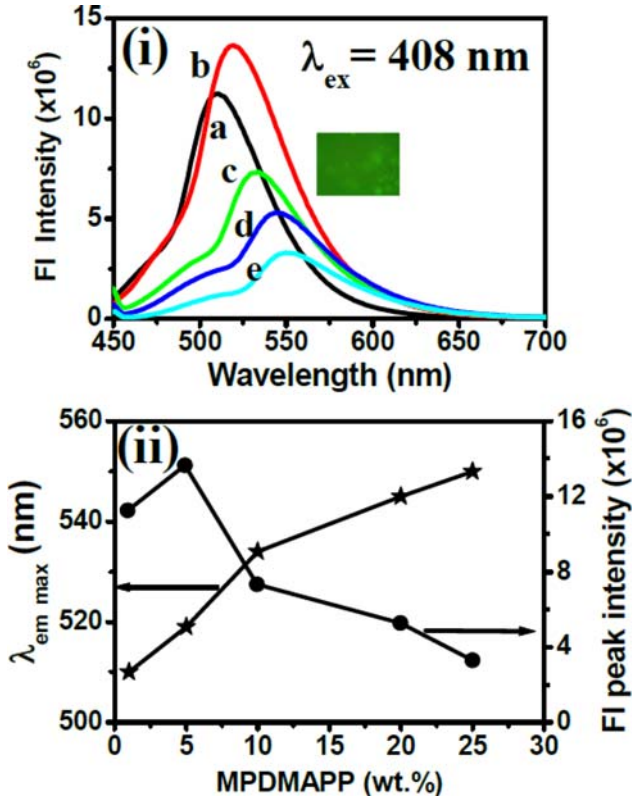

Figure 6. (i) Fluorescence emission spectra of (a) 1 wt %, (b) 5 wt %, (c) 10 wt %, (d) 20 wt %, (e) 25 wt % MPDMAPP doped PC for 408 nm excitation (inset: fluorescence microscopic image of the composite film emits green color emission under 450–480 nm excitation). (ii) The variation of fluorescence peak intensity and maximum emission peak wavelength as a function of MPDMAPP doping concentrations. [Color figure can be viewed in the online issue, which is available at wileyonlinelibrary.com.]

The emission band at 525 nm originates clearly from the polymer matrix of PC and this band exhibits a substantial decrease in intensity and an apparent red shift with the increase in dopant MPDMAPP fraction. This can be explained by the increase in absorption which acts as a filter to the luminescence (inner filter effect) although the front face geometry should help to minimize this effect. When the chromophore molecules are excited to singlet state, they eventually de-excite to the ground state either by fluorescence emission or by dissipating the excess energy by friction or momentum transfer to the polymer matrix. In defect-free chromophore-doped polymer composites, the nonradiative decay processes are less active since the rotational and vibrational motions of the molecules are hindered.[24] The MPDMAPP contains strongly electron donating dimethyl amino $N(CH_3)_2$ and methyl groups acting as donors and PC contains carbonate group, acting as acceptor, which are active site to form CTCs. The lone pair of nitrogen in the donor is transferred to the acceptor group to form a highly polar charge transfer state in which the excited state donor molecule sees a nearby acceptor molecule if the acceptor is within a distance of a few nanometers of the donor. Hence the donor molecule nonradiatively transfers its energy to the acceptor molecule.

The hydrophobic interaction also occurs between these groups, in addition to the dipole-dipole interaction between the carbonyl oxygen and carbonyl carbon of MPDMAPP with the carbonyl carbon of PC and *vice versa* as seen in the reaction scheme (Figure 2). The hydrophobic structures are found increasing with MPDMAPP concentration in PC, resulting in bathochromic shift of maximum fluorescence emission wavelength. Hence, the concentration-dependent shift in the fluorescence emission can be interpreted as the result of energy transfer between adjacent pairs of MPDMAPP chromophore molecules. The donor molecule of MPDMAPP in its electronic excited state may also transfer energy to an acceptor molecule through dipole-dipole coupling. This may be due to an increase in amorphous nature of the PC/MPDMAPP composites and increase in rigidity of the polymer matrix. Upon excitation in this restricted condition, the MPDMAPP chromophore molecules release their energy in the form of fluorescence after vibronic transitions. Beyond 5 wt % doping, the decrease in emission peak intensity as shown in the Figure 6(ii) is due to the increase in the probability of cross-relaxation process with smaller acceptor-donor distance, which leads to a high probability of energy transfer in which a loss of energy occurs. This causes the concentration quenching, which emits the fluorescence light with decrease in intensity, due to formation of nano-aggregated structure from isolated MPDMAPP chromophore molecules within PC as seen in TEM images.

Here, the energy transfer between identical chromophore molecules is known as quenching mechanism, which facilitates the energy migration.[25] This arises mainly due to the reduction in the available free volumes within the polymer matrix and the

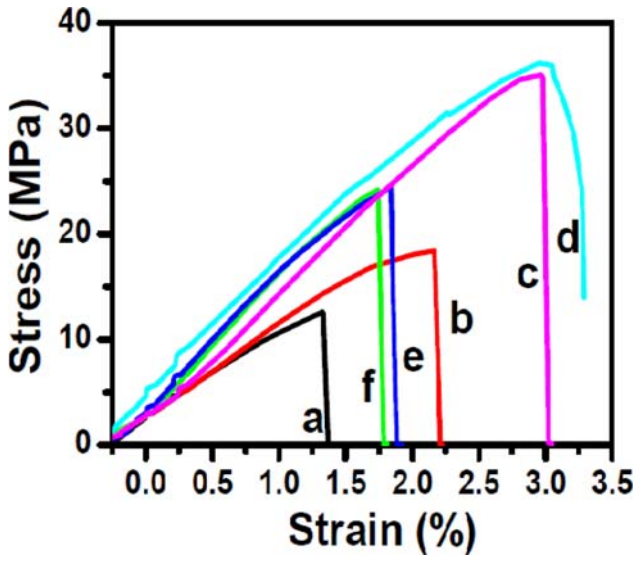

Figure 7. Stress–strain curves of (a) pure PC, (b) 1 wt %, (c) 5 wt %, (d) 10 wt %, (e) 20 wt %, and (f) 25 wt % MPDMAPP doped PC. [Color figure can be viewed in the online issue, which is available at wileyonlinelibrary.com.]

mobility of chromosphere molecules may restrict by suppressing the free volumes to prevent nonradiative transitions.[4,26] Hence, the rotational motion of $N(CH_3)_2$ groups of MPDMAPP are not feasible. However, with further increasing of doping concentration, there is also a decrease in spacing between the PC and MPDMAPP molecules and the possibility of nonradiative transfer of the carriers to MPDMAPP increases.[24–27] This phenomenon leads to a decrease in the fluorescence emission intensity at higher concentrations of MPDMAPP doped PC composites. These are competing effects, where the increase in fluorescence emission up to 5 wt % is due to enhanced excitation rate but which is then offset by the quenching of the emission intensity at higher doping concentration.[28–32] Hence, the increase in MPDMAPP doping in PC subsequently emits fluorescence with shift of 40 nm towards higher wavelength side in the green spectral region. The observed fluorescence microscopic images of the composite films illustrated in the inset of Figure 6(i) show the green light emission upon 450 to 480 nm excitation. In other words, the prepared PC/MPDMAPP composite films are photochromic in nature due to the photo-induced electron transfer reaction and can be used for color tuning applications.

Mechanical Studies

In order to check whether the mechanical properties of PC improved by adding MPDMAPP, the stress–strain curves of pure and PC/MPDMAPP composites with different concentrations were recorded and are shown in Figure 7. It is observed from the figure that both the stress and strain increase with increase in MPDMAPP concentration. The toughness K (J/g) of the pure and PC/MPDMAPP composites, which tells how much energy is needed to break the sample[33] are estimated by taking the area under the stress (σ) versus strain (ε) curve by using eq. (3).

$$K = \int_{\varepsilon=0}^{\varepsilon=\varepsilon_{max}} \left(\frac{\sigma}{\rho}\right) d\varepsilon \quad (3)$$

where σ is the stress (Pa), ε is the strain, and ρ is the density (g/m^3) and the estimated toughness data have also been given in Table I.

The mechanical properties of the composites are strongly dependent on the MPDMAPP content. It is observed that the increase in MPDMAPP content reflects as an increase in Young's modulus, toughness, tensile strength, and elongation at break up to 5 wt % and 10 wt %. Beyond this concentration, all these parameters decrease, whereas the stiffness reaches maximum values at highest MPDMAPP concentrations mainly due to homogeneous distribution of MPDMAPP particles in PC resulting into nanodomains.

The enhancement in rigidness of chains improves the mechanical strength of the PC/MPDMAPP nanocomposites. The decrease in mechanical properties beyond 10 wt % doping is probably due to agglomeration of MPDMAPP nanoparticles and as a result the composite films will become brittle in nature. These agglomerates can act as areas of localized reduced strength and defect sites that result in a general decrease in overall yield strength. Also the presence of voids near MPDMAPP and agglomerate surface could contribute to general decrease in yield strength at higher MPDMAPP loadings.

PALS and DBS Studies

The positron lifetime spectra of pure PC and PC/MPDMAPP composites showed three distinct lifetime components τ_1, τ_2, and τ_3 with relative intensities I_1, I_2, and I_3. The variations of lifetime components and their corresponding intensities as a function of MPDMAPP doping concentrations are shown in Figure 8. It is observed that the shortest lifetime component τ_1 and the intermediate lifetime component τ_2 increase in samples up to 5 wt % MPDMAPP and beyond it both lifetimes decrease slightly with increase in MPDMAPP doping concentration in PC. The longest component τ_3 is due to ortho-positronium (o-Ps) pick-off and corresponding intensity I_3 decreases continuously with increase in doping concentration. I_2 initially increases and then decreases slightly and again increases with increase in MPDMAPP concentration.

From these variations, it is understood that the addition of MPDMAPP in PC creates local lattice distortion and creates local negatively charged domains, which can strongly trap positrons.[6] The increase in I_2 and decrease in I_3 indicate the increasing number of trapped positrons with doping and reduction in o-Ps formation probability, due to increased electron density brought in by MPDMAPP.

In the present polymer composite, containing polar groups and complex structure, the probability of positronium formation is complex in nature and hence cannot be explained on the basis of free volume theory. Hence the variation of τ_3 and I_3 may be explained within the framework of spur model of o-Ps formation, as the o-Ps intensity depends on the probability of finding excess electrons. In this case, the Ps formation must compete with the other processes such as positron and electron scavenging,

Table I. Mechanical Properties of Pure and MPDMAPP Doped PC

MPDMAPP content (wt %)	Young's modulus (MPa)	Tensile strength (MPa)	Stiffness (N/m)	Elongation at fracture (%)	Toughness (J/g)
0 (pure PC)	995	12.61	24,511	1.36	11
1	974	18.42	28,015	2.19	26
5	1320	35.08	37,399	3.00	61
10	1578	36.20	24,986	3.29	77
20	1494	24.19	42,962	1.86	28
25	1129	24.47	41,861	1.76	26

positron and electron escaping from the spur etc., which reduce the Ps formation and reflected in a decrease in I_3.[34–37]

When the aromatic compounds (chalcone derivative) are added to polymers, the electrons can be scavenged by these aromatic compounds, mainly because of the formed CTCs (defects) which are expected to affect Ps formation (inhibition of o-Ps formation). In the process of chemical quenching, the o-Ps combines with the polar molecule to form a complex, and then it annihilates, such that the self-annihilation lifetime get reduced.[11–14] The chalcone chromophore MPDMAPP dopant contains a nitro functional group, i.e., dimethylamino $N(CH_3)_2$, which is expected to reduce the number of electrons available to the positron to form Ps.

In order to understand the inhibition effect further, the behavior of I_3 at different concentrations of MPDMAPP is related to $I_3^o/I_3 = 1 + K_{inhib}M$, where I_3^o is the o-Ps intensity of pure polymer without doping, K_{inhib} is called the Ps inhibition constant, and M is the doping concentration.[37,38] The value of inhibition constant $K_{inhib} = 0.05515\ mol^{-1}$ is obtained from the slope of I_3^o/I_3 versus MPDMAPP concentration (M) graph (with correlation coefficient $R = 0.99$) as shown in Figure 9(a) and confirms the inhibitor and electron scavenging behavior of MPDMAPP in PC. The continuous decrease in the o-Ps pick-off lifetime τ_3 with increase in MPDMAPP doping concentration as shown in Figure 8 is most probably due to the quenching effect on o-Ps, such as chemical quenching or spin conversion. Spin conversion of o-Ps is a process in which o-Ps exchanges its electron with another electron from the surface of the pore, which has an opposite spin, and then converts into p-Ps and annihilates just as p-Ps does.[12–14]

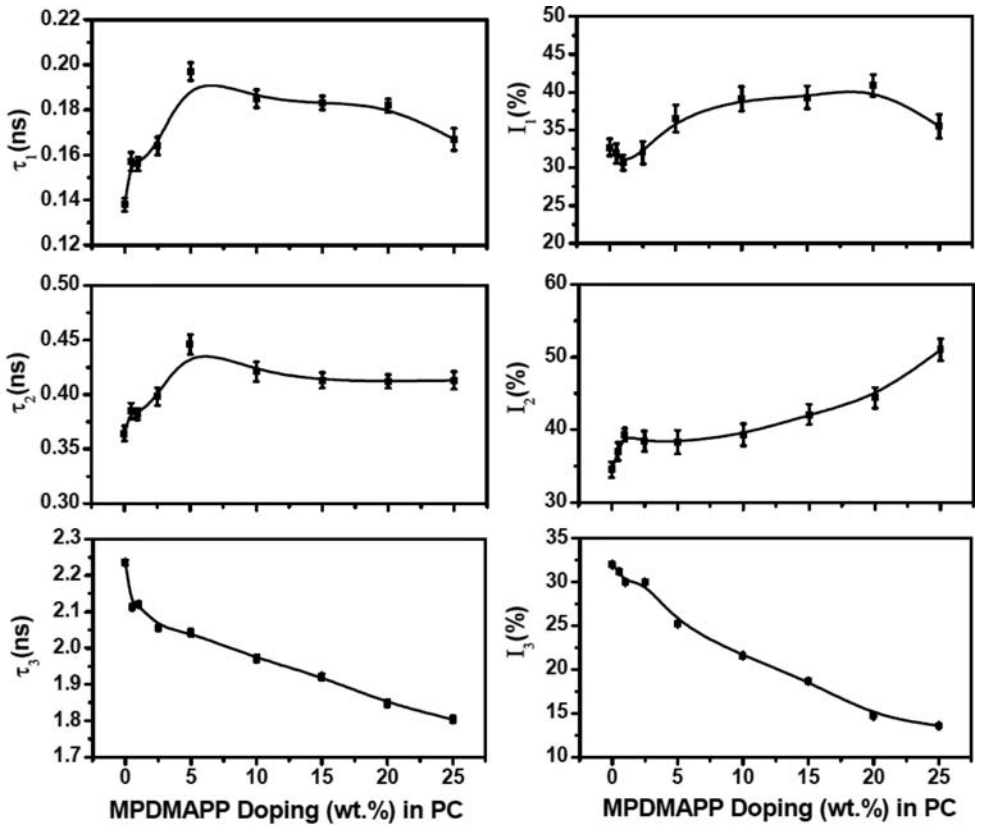

Figure 8. Variation of positron lifetimes τ_1, τ_2, and τ_3 and intensities I_1, I_2, and I_3 as a function of MPDMAPP doping concentration in PC.

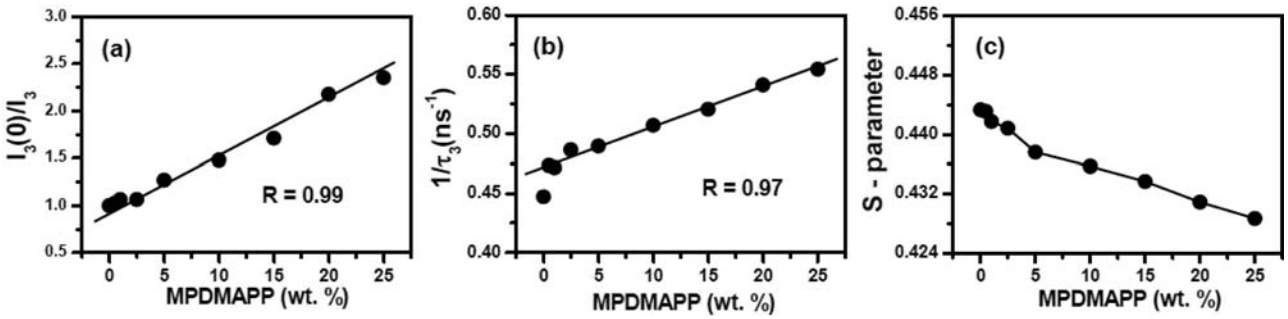

Figure 9. Variation of a) $I_3(0)/I_3$, b) $1/\tau_3$, c) *S*-parameter with MPDMAPP doping in PC.

The nitro functional group i.e., dimethylamino $N(CH_3)_2$, of the doped chromophore is known to be a strong quencher of o-Ps lifetime. The rate constant of chemical reaction between Ps and chromophore molecules can be expressed from the equation $\lambda_3 = \lambda_P + k_{Ps}[M]$, where λ_3 is reciprocal of the measured o-Ps lifetime (τ_3) at concentration $[M]$ and k_{Ps} is a measure of the chemical reactivity between the Ps and MPDMAPP in the polymer matrix.[38,39] From Figure 9(b), it is observed that the linear relationship of the plot of $1/\tau_3$ (λ_3) versus concentration of MPDMAPP in PC (with correlation coefficient $R = 0.97$) supports the above postulated Ps complex formation mechanism. The slope of this plot gives k_{Ps} value of 0.00364 mol^{-1} ns^{-1} for MPDMAPP in PC. Hence it is clear that both the o-Ps inhibition and quenching of Ps formation occur in PC/MPDMAPP composite.

The measurements of Doppler broadening of the positron annihilation gamma ray line shape are helpful in monitoring the changes of the predominant trapping sites for positrons in doped polymer.[15,36,37] The S-parameter from DBS spectrum is defined as the ratio of counts in selected number of channels around the peak to the total number of counts under it and thus represents the fraction of positrons annihilating with low momentum electrons. The variation of the *S*-parameter as a function of

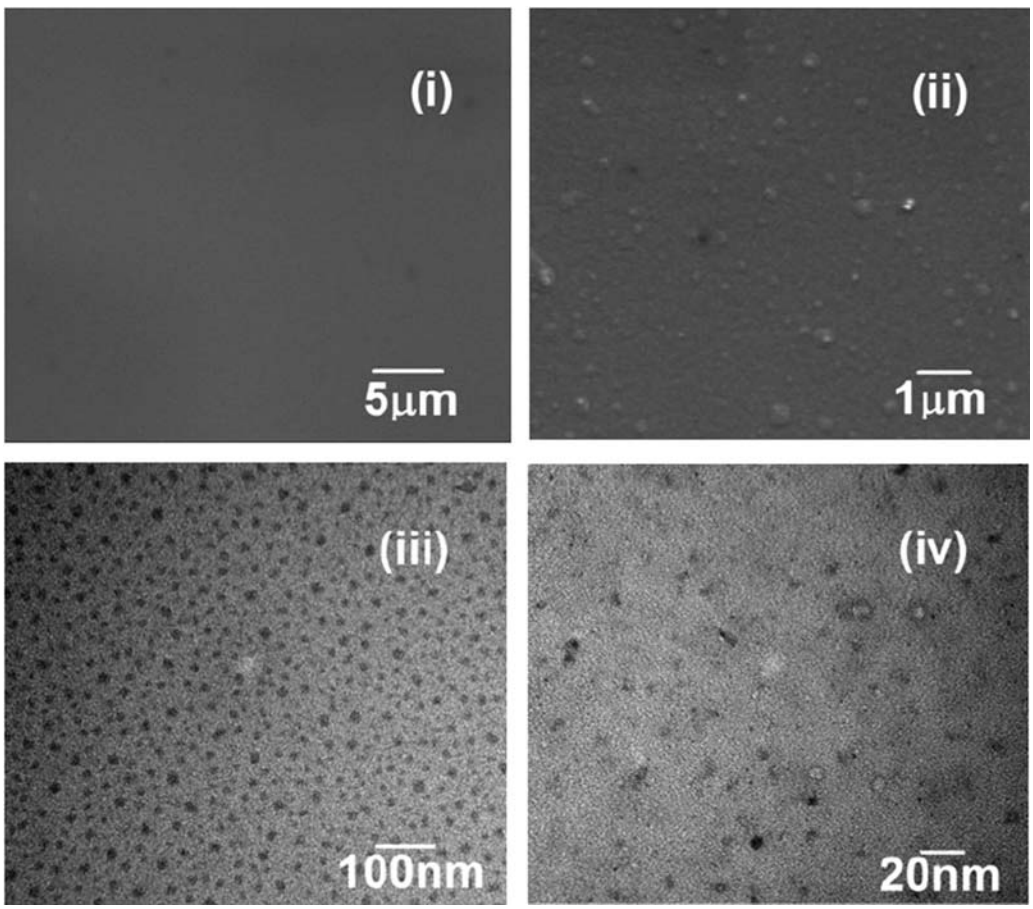

Figure 10. SEM images of (i) pure PC and (ii) 10 wt % MPDMAPP doped PC and TEM images of (iii) 5 wt % and (iv) 10 wt % MPDMAPP doped PC composite films.

MPDMAPP doping concentration in PC is shown in Figure 9(c). The *S*-parameter continuously decreases with increase in doping concentration and hence indicates the reduction of defect concentration. The reduction in *S*-parameter in this case is also due to the strong quenching and inhibition of Ps.

SEM and TEM Analysis

The SEM and TEM images of the PC/MPDMAPP composite films are given in Figure 10. The SEM image of pure PC film displays a smooth and homogeneous surface [Figure 10(i)]. The SEM image of MPDMAPP doped PC clearly shows a well and uniform dispersion of MPDMAPP nanocrystalline structures in PC matrix [Figure 10(ii)]. The smooth surface of pure PC is transformed into a little rough for 10 wt % MPDMAPP doping in PC and it insures maximum surface area for strong interaction with the absence of pores and has no other interface layer indicating the complete miscibility and amorphous nature of the composite. The formation of homogeneous composite is due to interactions between the functional groups of PC and MPDMAPP.

The growth of nanostructures of MPDMAPP within PC films was examined with TEM images. The TEM image of 5 wt % doped PC/MPDMAPP composite films shows good dispersion of synthesized chalcone derivative MPDMAPP nanostructures within PC with uniform size of 5 to 10 nm [Figure 10(iii)]. The TEM image of 10 wt % MPDMAPP doped PC shows that the size of MPDMAPP nanostructures increases to 10 to 15 nm with increase in doping level and shows amorphous structures [Figure 10(iv)]. No agglomeration was observed, indicates the strong interaction between MPDMAPP dopant and PC. Hence the green emission of the PC/MPDMAPP composites as seen in fluorescence studies is due to the growth of the nanostructures.

SUMMARY AND CONCLUSIONS

The conclusions drawn from this study are as follows. The polymer PC embedded with chalcone derivative MPDMAPP composite films were prepared using solution casting. The interaction between the PC and MPDMAPP was confirmed from FT-IR results. The optical band gap decreases with increase in MPDMAPP concentration. The composite films show good optical photochromic property. The decrease in fluorescence intensity supported the findings from positron annihilation studies. The o-Ps inhibition in PC/MPDMAPP composites was investigated using both positron lifetime and Doppler broadening measurements. The decrease in both o-Ps intensity I_3 and the *S*-parameter with increase in MPDMAPP doping clearly indicated both inhibition of o-Ps formation and Ps quenching in this particular composite. The XRD results show an increase in amorphous nature. The prepared PC/MPDMAPP composites are mechanically high strength films, as observed by increase in Young's modulus, tensile strength, and stiffness up to 10 wt % doping. The SEM images show a smooth surface for pure PC which got converted into a little rough for 10 wt % MPDMAPP doping and indicated complete miscibility and amorphous nature of the composite. The growth of nanostructures of MPDMAPP within PC films observed in TEM images confirms the uniform dispersion and bonding between the functional groups of PC and MPDMAPP.

The authors are thankful to University Grants Commission (UGC) for the financial assistance in the form of research project (F.36-165/2008(SR)/2009), Department of Atomic Energy, Board of Research in Nuclear Sciences (BRNS) (2010/37C/7/BRNS/832), and Department of Science and Technology (DST) Government of India (SR/FTP/PS-011/2010). One of the authors (T.S.) is thankful to Mangalore University for the award of Ph.D. Research Fellowship. The authors are further thankful to Prof. R. Somashekar, Department of Physics, University of Mysore for providing the XRD facility and to Prof. Vincent Crasta, Department of Physics, St. Joseph Engineering College, Mangalore, for providing chalcone derivative sample. The authors are thankful to SAIF Chennai, SAIF Cochin, and SAIF Chandigarh for fluorescence, SEM and TEM measurements. The authors of this manuscript are Ms. T. Sheela, who is doing Ph.D. under R.F. Bhajantri's supervision, carried out the research work such as preparation of composite films, characterization of the samples using FT-IR, fluorescence, UV–Vis spectrophotometers, and analysis of the results. Dr. P.M.G. Nambissan provided the PALS and DBS data and analysis of these results. Dr. V. Ravindrachary involved in the interpretations of PALS and other results. Mr. Sunil G. Rathod is also R.F. Bhajantri's student doing Ph.D., involved in characterization works such as XRD and mechanical measurements of the samples. Dr. Boja Poojary helped in chemical works such as sample preparation methods and analysis of FT-IR and fluorescence results.

REFERENCES

1. Djurisic, A. B.; Guo, W. L.; Li, E. H.; Lam, L. S. M.; Chan, W. K.; Adachi, S.; Lu, Z. T.; Kwok, H. S. *Opt. Commun.* **2001**, *197*, 355.
2. Bhajantri, R. F.; Ravindrachary, V.; Poojary, B.; Ismayil, A.; Harisha, A.; Vincent, C. *Polym. Eng. Sci.* **2009**, *49*, 903.
3. Tu, Y.; Zhang, Q.; Agren, H. *J. Phys. Chem. B* **2007**, *111*, 3591.
4. Bhajantri, R. F.; Ravindrachary, V.; Harisha, A.; Ismayil, A.; Ranganathaiah, C. *Phys. Status Solidi C* **2009**, *6*, 2429.
5. Kunzelman, J.; Kinami, M.; Crenshaw, B. R.; Protasiewicz, J. D.; Weder, C. *Adv. Mater.* **2008**, *20*, 119.
6. Ravindrachary, V.; Ismayil, A.; Nayak, S. P.; Dutta, D.; Pujari, P. K. *Polym. Degrad. Stab.* **2011**,*96*, 1676.
7. Jang, B. N.; Wilkie, C. A. *Polym. Degrad. Stab.* **2004**, *86*, 419.
8. Jaya Vani, S.; Mohanty, S.; Parvaiz, M. R.; Nayakm, S. K. *Macromol. Res.* **2011**, *19*, 563.
9. Bernadette Higgins, A.; Brittain, W. *J. Eur. Polym. J.* **2005**, *41*, 889.
10. Mukherjee, M.; Chakravorty, D.; Nambissan, P. M. G. *Phys. Rev. B* **1998**, *57*, 848.
11. Sharma, S. K.; Pujari, P. K.; Sudarshan, K.; Dutta, D.; Mahapatra, M.; Godbole, S. V.; Jayakumar, O. D.; Tyagi, A. K. *Solid State Commun.* **2009**, *149*, 550.

12. Zhang, R.; Robles, J.; Kang, J.; Samha, H.; Chen, H. M.; Jean, Y. C. *Macromolecules* **2012**,*45*, 2434.
13. Dlubek, G.; Taesler, C.; Pompe, G.; Pionteck, J.; Petters, K.; Redmann, F.; Krause-Rehberg, R. *J. Appl. Polym. Sci.* **2002**, *84*, 654.
14. Harms, S.; Ratzke, K.; Pakula, C.; Zaporojtchenko, V.; Strunskus, T.; Egger, W.; Sperr, P.; Faupe, F. *J. Polym. Sci. Part B: Polym. Phys.* **2011**, *49*, 404.
15. Hunt, A. W.; Cassidy, D. B.; Sterne Pm, A.; Cowan, T. E.; Howell, R. H.; Lynn, K. G.; Golovchenko, J. A. *Phys. Rev. Lett.* **2001**, *86*, 5612.
16. Bertolaccini, M.; Zappa, L. *Nuovo Cimento. B* **1967**, *52*, 487.
17. Olsen, J. V.; Kirkegaard, P.; Pedersen, N. J.; Eldrup, M. *Phys. Stat. Sol. C* **2007**, *4*, 4004.
18. Hakimelahi, H. R.; Hu, L.; Rupp, B. B.; Coleman, M. R. *Polymer* **2010**, *51*, 2494.
19. Crasta, V.; Ravindrachary, V.; Bhajantri, R. F.; Naveen, S.; Shridar, M. A.; Shashidhara Prasad, J. *Proc. SPIE* **2005**, *5935*, 1.
20. Dwivedi, Y.; Singh, A. K.; Prakash, R.; Rai, S. B. *J. Lumin.* **2011**, *131*, 2451.
21. Tauc, J.; Grigorovici, R.; Vancu, A. *Phys. Status Solidi* **1966**, *15*, 627.
22. Davis, E. A.; Mott, N. F. *Philos. Mag.* **1970**, *22*, 903.
23. Ravindrachary, V.; Praveena, S. D.; Bhajantri, R. F.; Ismayil, V. C. *AIP Conf. Proc.* **2013**, *1512*, 126.
24. Yu, H.; Zi, W.; Lan, S.; Gan, S.; Zou, H.; Xu, X.; Hong, G. *Opt. Laser Technol.* **2012**, *44*, 2306.
25. Hennig, A.; Hatami, S.; Spieles, M.; Resch-Genger, U. *Photochem. Photobiol. Sci.* **2013**, *12*, 729.
26. Meyer, E. F.; Jamieson, A. M.; Simha, R.; Palmen, J. H. M.; Booij, H. C.; Maurer, F. H. *J. Polymer* **1990**, *31*, 243.
27. Gagandeep, K.; Rai, S. B. *J. Phys. D: Appl. Phys.* **2011**, *44*, 425306.
28. Aldred, M. P.; Chong, L.; Guo-Feng, Z.; Wen-Liang Alexander, G. G.; Li, D. Q.; Dai, Y.; Dongge, M.; Ming-Qiang, Z. *J. Mater. Chem.* **2012**, *22*, 7515.
29. Li, G.; Liu, S.; Chu, Z.; Gao, H.; Wu, D.; Cui, J.; Yue, D.; Wang, Z. *J. Lumin.* **2012**, *132*, 2961.
30. Jadhav, A.; Pawar, A.; Hwang, T. R.; Lee, J. W.; Choi, M. W.; Kim, B. K.; Kang, Y. S. *Polym. Int.* **2012**, *61*, 943.
31. Wang, P.; Zhao, X.; Li, B. *Nano Energy* **2012**, *1*, 152.
32. Qi, C.; Zhang, C.; Jiang, B.; Wang, X.; Liu, Y. J.; Cao, Y.; Xiao, M. *Opt. Expr.* **2012**, *20*, 9135.
33. Morimune, S.; Nishino, T.; Goto, T. *Appl. Mater. Interfaces* **2012**, *4*, 3596.
34. Hirata, K.; Kobayashi, Y.; Ujihira, Y. *J. Chem. Soc. Faraday Trans.* **1997**, *93*, 139.
35. Wang, C. L.; Kobayashi, Y.; Zheng, W.; Zhang, C.; Nagai, Y.; Hasegawa, M. *Phys. Rev. B* **2001**, *63*, 064204.
36. Ramya, P.; Guagliardo, P.; Pasang, T.; Ranganathaiah, C.; Samarin, S.; Williams, J. F. *Phys. Rev. E* **2013**, *87*, 052602.
37. Huang, C. M.; Hellmuth, E. W.; Jean, Y. C. *J. Phys. Chem. B* **1998**, *102*, 2474.
38. Mohamed, H. F. M.; Ito, Y.; Ali, M. A.; El-Sayad, E.; Abdel-Hady, E. E. *Polymer* **1996**, *37*, 1529.
39. Siegel, R. W. *Annu. Rev. Mater. Sci.* **1980**,*10*, 393.